

Research



Cite this article: Borin D. 2020 Targeted patterning of magnetic microparticles in a polymer composite. *Phil. Trans. R. Soc. A* **378**: 20190256.
<http://dx.doi.org/10.1098/rsta.2019.0256>

Accepted: 17 November 2019

One contribution of 18 to a theme issue
'Patterns in soft and biological matters'.

Subject Areas:

materials science, fluid mechanics

Keywords:

magnetic polymer, controllable anisotropy,
magnetic structuring

Author for correspondence:

Dmitry Borin

e-mail: dmitry.borin@tu-dresden.de

Targeted patterning of magnetic microparticles in a polymer composite

Dmitry Borin

Institute of Mechatronic Engineering, Chair of
Magnetofluidynamics, Measuring and Automation
Technology, Technische Universität Dresden, 01062 Dresden,
Germany

 DB, 0000-0003-3842-1487

Structured and polymerized in a uniform external magnetic field, polymer composites based on magnetic soft microparticles are considered. Variations of magnetic field parameters and material composition provide a possibility of targeted microstructural patterning of these composites. The influences of parameter variations on the resulting internal micro-structure of the low concentrated specimens are evaluated and visualized using optical microscopy and microcomputed tomography. The experimental findings are discussed in order to provide advanced possibilities of controlled patterning of soft magnetic materials. It is experimentally demonstrated that the final three-dimensional morphology of composite structure is determined mainly by the concentration of magnetic powder. The intensity of the applied magnetic field influences the rate of structuring of particles in initially viscous media and, therefore, may provide a potential opportunity to obtain non-ergodic microstructures when the matrix is polymerized before the particles have completed the structuring process. The results obtained can serve as a basis for further development of the engineering method of targeted patterning. The method is intended to obtain a material with the desired microstructure by selecting specific parameters of external stimuli and components of the composite.

This article is part of the theme issue 'Patterns in soft and biological matters'.

1. Introduction

The magnetic field-induced anisotropy of the microstructure of soft matters such as magnetic suspensions, gels and elastomers can be used to remotely and actively tailor their physical properties. In the case of stable ferrofluids and magnetorheological suspensions, the formation of aggregates of magnetic nano- and microparticles is reversible and primarily leads to changes in their rheological behaviour [1]. In cross-linked gels and elastomers, the structuring is limited due to restricted particle mobility in the matrix. On the other hand, these elastic materials are in a liquid state before the curing process. Thus, they can be structured by an external magnetic field applied before and during the curing process. In that case, the matter refers to composites which are initially anisotropic, i.e. they are anisotropic without externally applied stimuli after they were manufactured. Figure 1 shows an example of real three-dimensional microstructure of an isotropic (*a*), i.e. not patterned, and anisotropic (*b*), i.e. patterned, polymeric composite based on nickel microparticles. Such systems attract the attention of researchers both from an applied and fundamental point of view, including basic, engineering and bio-medical applications, e.g. [1–4].

Field-induced particle structuring in liquid and elastic matrices and its effect on the materials' field response have been studied in the past and are still under intensive theoretical and experimental investigations [1,2,4]. The well-known microscopic approaches of the rheological behaviour of magnetic suspensions are based on the concept of either chain-like or dense column-like aggregates formed by the particles [1,5,6]. The size and shape of these aggregates are determined by the combination of the forces of magnetic attraction between the particles and viscous forces in the carrier liquid destroying the aggregates. Theories, based on these concepts, lead to different dependencies of the macroscopic stress on the global rate of the composite deformation and can provide realistic prediction of the material behaviour. However, the chain model is rather a very simplified approach suitable for very diluted systems. In fact, the morphology of particle structures depends on various physical parameters and may differ significantly from simple chains. Optical microstructural observations have shown that particles in magnetorheological suspensions build thick columnar aggregates and more complicated structures oriented in the direction of the applied field [2]. Moreover, recently it was experimentally shown, using a microchannel filled with a low concentrated magnetic fluid, that geometrical parameters of the particle structures depend not only on the strength but on the duration of the applied magnetic field as well [7]. With increasing duration and strength, the size of the structures increases. This generally corresponds with results of the known theoretical analysis and computer simulations [8–10] as well as observations performed for very diluted magnetorheological fluids [11]. In terms of particle structuring dynamics in magnetorheological fluids, two processes are distinguished: the initial formation of thin chains after the field was applied and further formation of thicker aggregates [8]. The duration of the second process reaches a couple of minutes.

As already mentioned above, soft magnetic elastic composites in the non-polymerized state represent a kind of magnetorheological suspension. When external magnetic field is applied to the suspension, formation of particle structures should occur similar to the magnetic fluid way. There are microscopic based predictions of the magnetic and magneto-mechanical response of structured soft magnetic elastic composites accounting for the linear chain-like aggregates, e.g. [12,13]. Nevertheless, the criteria of transition from the chain like to the bulk structures as well as the mechanism of the aggregate formation and destruction have not been developed up to now. From an experimental point of view, various particle morphologies can be observed in the cross-linked composites under external magnetic fields. It has been demonstrated in several studies that microcomputed tomography (μ CT) is an excellent tool to provide three-dimensional structural information about not highly concentrated composite materials based on magnetic microparticles, e.g. [4,14–18]. This method yields a three-dimensional map of the sample internal structure due to the X-ray contrast between particles and matrix. Modern X-ray tomography equipment enables

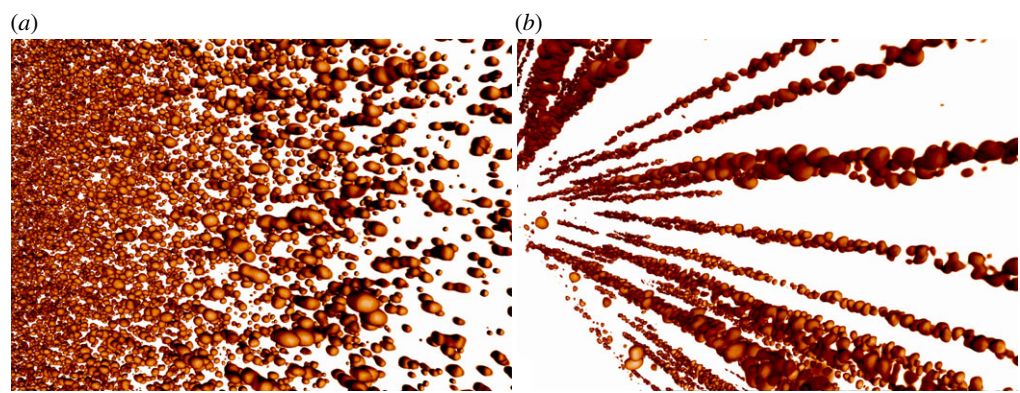


Figure 1. Real three-dimensional microstructure of a non-patterned (a) and patterned (b) magnetic polymer containing nickel microparticles (figure 3). Images are obtained using computed microtomography as described in the article. Without scale. (Online version in colour.)

spatial resolution down to a few micrometres allowing separation and identification of single magnetic particles inside the composite. For instance, in [16], the influence of the concentration of magnetic powder on the final structure of the produced composites was studied. It has been shown that any variation of the particle concentration results in a completely different morphology: from homogeneous distribution of particle columns (samples with the lowest fraction of magnetic powder) to specimens with particle columns, which are self-assembled and more complex aggregates with their longitudinal axis parallel to the magnetic field. The influence of the magnetic field strength on the final particle chains morphology was studied in [15]. It has been observed that appearance of the single chains is a feature of very low concentrated systems and is stimulated by weak magnetic fields. According to obtained results, the number of chains formed in the material increases with decreasing field strength while vice versa the diameter of the structures becomes larger with increasing field strength. There is a similarity with a structuring observed in magnetorheological suspensions. Apart from the chain-like and cylindrical dense structures, other kinds of particle aggregates can appear in non-concentrated magnetic composites under influence of an externally applied magnetic field. These aggregates can have various morphologies such as sheet-like, tube-shaped and canyon- or net-like structures and are long-living [14,16,18]. In a recent study non-ergodic tube-like structures were under investigation [18]. From a theoretical point of view, the thermodynamic equilibrium state of the diluted and structured magnetic composite must correspond to whole cylinders without the central cavity. However, non-equilibrium structures, which stably exist for a long time, have been observed. A critical issue that has not been addressed in the above-mentioned studies, is the fact the rheological properties of the carrier medium are changing during polymerization together with a change in a composite's microstructure. The process of polymerization of silicone composites is initiated by the addition of a chemical catalyst and actually begins before the magnetic field for structuring the powder particles has been applied. Thus, in this case, it is inappropriate to speak about targeted and precisely controlled structuring of composites. As was briefly noted in [14], the specimen, which required a much longer time for hardening, has a different morphology comparing to the faster cross-linked one. In the current study, we analysed the microstructure of rigid magnetic polymers of various compositions, which were structured in an externally homogeneous magnetic field and then polymerized by ultraviolet radiation. This approach allows the process of polymerization to be initiated at a given point in time, providing a possibility of the targeted patterning of composites. Obtained structures are visualized using microscopy and μ CT methods. The article is organized as follows. At first, the basic physical principles of structuring particles in a viscous medium due to magnetic dipole interaction are given. Next, the used materials and experimental methods are presented. The main part of the

article is devoted to the discussion of the obtained patterns and their visualization. It concludes with a short summary and outlooks.

2. Background

Microparticles of a magnetic polymer are suspended in an initially liquid medium. When the medium stays permanently liquid, the process of structuring can be described using classical methods of the theory of phase transitions and heterogeneous fluctuation. External magnetic field \mathbf{H} induces in the particle with a radius r a magnetic dipole moment parallel to the field vector

$$\mathbf{m} = \frac{4}{3} \pi r^3 \chi \mathbf{H}, \quad (2.1)$$

where χ is the magnetic susceptibility, which can be defined as

$$\chi = 3 \frac{\mu_p - \mu_c}{\mu_p + 2\mu_c}, \quad (2.2)$$

where μ_p is the magnetic permeability of the particle and μ_c is the magnetic permeability of the liquid carrier medium [19]. The permeability χ can be considered equal to 3 for composites based on typical magnetic microparticles, since the ratio of the magnetic permeability of the particle material to the permeability of the carrier media is much greater than unity [2].

Considering two particles as point dipoles with the same induced moment \mathbf{m} directed parallel to the applied field \mathbf{m} and separated by the distance R (figure 2), one calculates the energy of interparticle interaction as

$$W = \frac{\mu_0 \mu_c m^2}{4\pi R^3} (1 - 3 \cos^2 \alpha), \quad (2.3)$$

where the α is the angle between the field \mathbf{H} and the line connecting the particle mass centres.

When the particles are oriented in the field direction and in contact (figure 2), equation (2.3) can be written as

$$W(R = 2r, \alpha = 0) = \frac{\mu_0 \mu_c m^2}{32\pi r^3}. \quad (2.4)$$

The structure formation upon stimulus of a homogeneous field is governed by ratios of the interparticle magnetic forces to the Brownian and hydrodynamic forces. For a quiescent liquid, it is defined solely by the ratio of the interparticle force to the Brownian force

$$\lambda = \frac{\mu_0 \mu_c m^2}{16\pi r^3 k_B T}, \quad (2.5)$$

where μ_0 is the permeability of free space, k_B is the Boltzmann constant and T is the absolute temperature. Thus, the structuring in the applied field will occur if the ratio λ , also called the interaction parameter, is greater than 1.

It should be noted that for particles with high magnetic permeability it may be necessary to take into account the multipolar interaction. Moreover, since each magnetized particle creates its own field, the local field effect will also influence the dipole moment.

Neglecting the Brownian fluctuations of microparticles, the equation of motion for two particles attracted as a result of magnetic dipole interaction in the medium with viscosity η is

$$M \frac{d^2 R}{dt^2} + 6\pi \eta r \frac{dR}{dt} + \frac{3\mu_0 \mu_c m^2}{\pi R^4} = 0, \quad (2.6)$$

where M is the mass of the particle.

Assuming that the particles are oriented in the field direction and initially at rest at a distance of R from each other, we can estimate the time it takes them to move to the point of contact, that is in the position $R = 2r$. When integrating equation (2.6) the inertia can be neglected, because it is

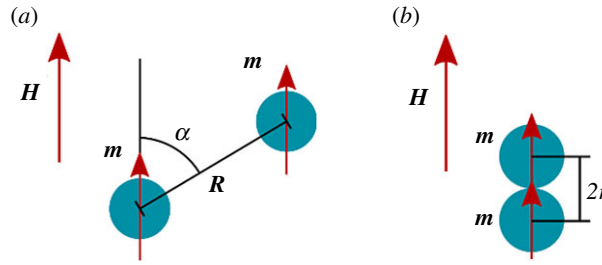


Figure 2. Magnetic dipole particles in the external magnetic field: particles separated by R distance from each other (a); particles in contact (b). (Online version in colour.)

several orders of magnitude smaller than the other terms. Thus, we get the following expression for time t :

$$t = \frac{6\pi^2\eta r}{15\mu_0\mu_c m^2} (R^5 - (2r)^5). \quad (2.7)$$

The initial distance between the particles is determined by their size and their volume concentration ϕ in the composite, which is

$$\phi = \frac{n\frac{4}{3}\pi r^3}{V}, \quad (2.8)$$

where V is the volume of the specimen and n the number of the particles with radius r in volume V . Assuming that the particles are distributed in the carrier medium initially homogeneously, it is possible to estimate the average initial distance between them as

$$R_0 \sim \left(\frac{V}{n}\right)^{1/3} \sim 2r \left(\frac{1}{\phi}\right)^{1/3}. \quad (2.9)$$

Taking $R = R_0$ in equation (2.7), it is possible to estimate the minimum time of aggregation of dipole particles in a viscous medium depending on the applied field and at a given concentration of the composite. Considering that $m \sim r^3$ (see equation (2.1)) and $\mu_p/\mu_c \gg 1$, we obtain that time t depends on the magnetic field strength, viscosity of the carrier medium and volume concentration of particles. That is, the size of the particles influences the structuring time only through the expression (2.8).

The formation of single chains of magnetic particles due to the dipole interaction is the first stage of magnetic patterning. As has been shown previously, complex structures are the result of further interaction of chains with both individual particles and each other, e.g. [2,8,20,21]. In the equilibrium state, the morphology of these complex structures is still determined by the particle volume concentration ϕ and the interaction parameter λ . Therefore, we consider below only the above basic parameters λ , ϕ and t as characteristic values for the samples under study. However, it should be noted that the statements considered are valid for systems of monodisperse identical spheres, while the real composites are based on polydisperse powders with particles of diverse shapes. Moreover, the actual concentration of the filler in the samples may differ from the desired concentration specified during their manufacture. Taking this into account, these basic parameters should be considered as estimates.

3. Material and methods

(a) Magnetic particles

Three types of magnetic powder were used as magnetic filler for the studied composites. Figure 3 shows the images of powder particles obtained with the Euromex ME.2660 microscope in the reflected light mode. Parameters of powders are given in table 1. Evaluation of the magnetic

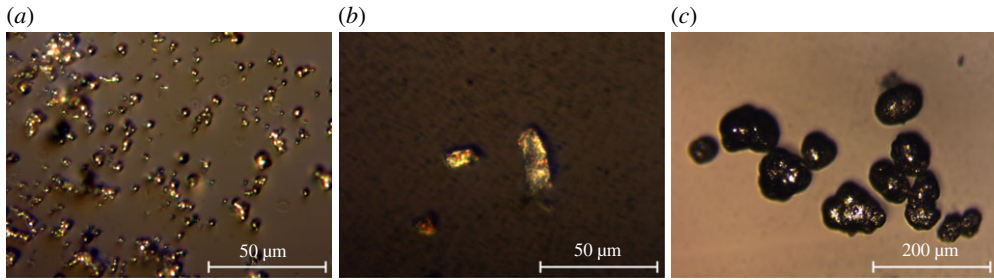


Figure 3. Microscopic images of used magnetic particles: BASF CC carbonyl iron (a); Höganäs ASC300 iron powder (b); Alfa Aesar Ni powder (c). (Online version in colour.)

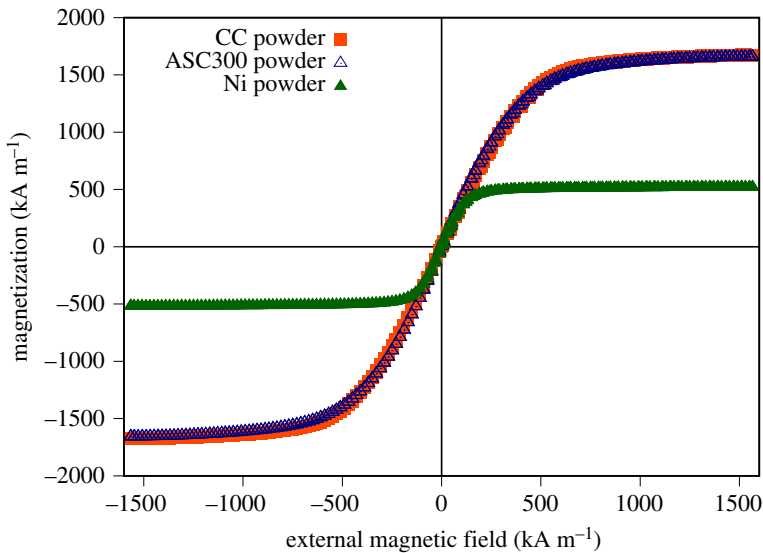


Figure 4. Magnetization curves of powders: the pressed powder was measured, and the weight and density of the powder material was taken into account when calculating the magnetization from the measured magnetic moment. (Online version in colour.)

Table 1. Parameters of used magnetic powders.

type	material	particle shape	average particle size
BASF CC powder	carbonyl iron	spherical	~ 5 μm
Höganäs ASC300 powder	iron	irregular	~ 45 μm
Alfa Aesar nickel powder	nickel	nearly spherical	~ 70 μm

properties of powders was carried out on the basis of the magnetization curves obtained experimentally using vibrating sample magnetometer Lake Shore 7407. Measured curves are given in figure 4. All powders are magnetic soft and the main difference is the higher saturation magnetization for iron-based powders. The initial magnetic susceptibility of powders (slope of the initial linear curve) is relatively the same.

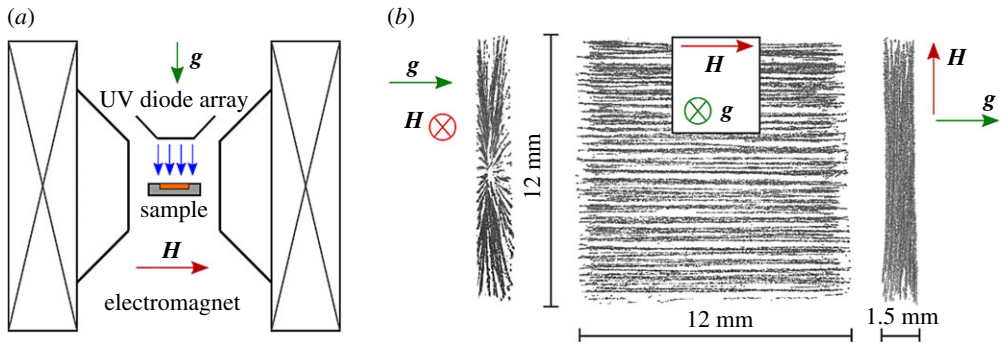


Figure 5. Schematic of the set-up for specimen fabrication (a) and views of the structured sample on three sides (left-hand view, top view and front view) with corresponding indication of the magnetic field H and gravity g directions (b). (Online version in colour.)

(b) Polymeric matrix

Clear UV resin R3 for bulk products (Research&Production Group Spektr, Russia) made of oligourethane methacrylates was used as a matrix. The initial viscosity of the resin, i.e. before curing, was measured with the Anton Paar MCR301 rotational rheometer at $T = 23^\circ\text{C}$ with a cone-plane geometry at shear rates in the range of $1\text{--}100\text{ s}^{-1}$. The resin is a Newtonian liquid in the considered range of shear rates with a viscosity of $\eta = 9.77\text{ Pa s}$. According to the resin manufacturer's data, UV irradiation (in the range of UV of 320–380 nm) of the sample within a few minutes is sufficient for full curing.

(c) Sample fabrication

The magnetic powder and liquid matrix in the given weight fractions (up to approx. 11 wt%) were mechanically mixed in the laboratory glass and vacuumized in order to remove air inclusions from the suspension. The resulting mixture was poured into a non-magnetic mould (PTFE) with plate-like geometry with a size of $12 \times 12 \times 1.5\text{ mm}$. Then the form was placed between the poles of the Bruker B-E25 electromagnet, so that the magnetic field generated by it was parallel to the sample plane (figure 5). The homogeneity of the magnetic field in the area where the sample was located was not less than 99%. The source of ultraviolet radiation (diode array) was placed perpendicular to the sample plane above the mould. The gravity was directed vertically downwards perpendicular to the sample plane and the magnetic field direction. The procedure for switching on the magnetic field and the radiation source as well as the concentration of the magnetic filler in the sample and the applied field strength were varied according to the task of obtaining a composite with a certain particle pattern. All treatments were performed at $T = 23^\circ\text{C}$.

(d) Microstructure visualization

For visualization of the microstructure of the fabricated samples, optical microscopy and computer microtomography were used. Optical observations of the surface of the obtained samples were carried out using an ME.2660 polarizing microscope (Euromex, The Netherlands) in a reflected light mode. Calibration of the scales was performed using a stage micrometre (Präzisionsoptik Gera, Germany). Digital images were recorded by a Carl Zeiss AxioCam CCD camera and processed with the ZEN 2 software package (Carl Zeiss, Germany). Tomographic investigations were conducted using the TomoTU set-up [22]. Projection images were generated with an angular increment of 0.25° with an acceleration voltage of 90 kV. CT-reconstruction process was performed calculating a three-dimensional model from the individual radiographs

by a software package developed at the TU Dresden. Digital image processing was carried out using the software packages ImageJ and VG Studio Max (Volume Graphics GmbH).

4. Targeted patterning

(a) Evaluation of key parameters

The interaction parameter λ (equation (2.5)) is determined by the particle size and the applied magnetic field strength and $\lambda \gg 1$ for all types of particles used, even in very small fields. The minimum field used in this work was 10 kA m^{-1} , and the maximum 450 kA m^{-1} , hence the interaction parameter was in the range $10^6 < \lambda < 10^{13}$. In this way, all the particles could be involved in the structuring process. Note that we do not take into account the influence of the geometric demagnetizing factor on the effective magnetic field. Firstly, all the specimens have the same geometry, and, secondly, for the particle concentrations we use, the influence of the macroscopic demagnetizing field can be negligible as shown in [23]. In accordance with equations (2.7)–(2.9), the key role in the dynamics of the structuring process is provided by the concentration of particles (initial distance between them), the strength of the magnetic field and the viscosity of the carrier medium. Since the initial viscosity of the matrix remained a constant parameter, the structuring time is controlled by a variation of the other two parameters. Dependence of structuring time t on the volume concentration of particles in the sample are shown in figure 6 for three different magnetic field strengths. These dependencies are the same for all types of magnetic filler used, as follows from equation (2.7). The use of powders of different types actually allows one to vary the number of particles per unit volume because of their different sizes and thus allows for a possible additional impact on the morphology of the particle aggregates. On the other hand, it is obvious that the size of particles cannot be neglected in terms of gravitational stability. The use of smaller particles is preferable in terms of their possible sedimentation over time. The use of large microparticles, however, provides an advantage in terms of the quality of the μCT -images obtained. In this context, figure 7 represents reconstructions of μCT -images of three samples with the same concentration of BASF CC carbonyl iron powder ($\phi \sim 0.15 \text{ vol.}\%$) with the average particle size of approximately $5 \mu\text{m}$. The samples are structured in various fields and therefore have different patterns (see discussion below). However, due to the small particle size comparable to the resolution of the measurement method, we will avoid a direct comparison of three-dimensional microstructure morphology for these composites. Similar to larger particle samples, a composite, structured in a higher magnetic field (figure 7c) and with the same filler volume concentration, contains fewer aggregates and they are thicker than aggregates in a composite structured in a weaker field (figure 7d). Although the statement about the difference in the number of elongated aggregates for the samples presented in figure 7b,c is quite obvious (see as well figure 8), it is impossible to conclude correctly about their thickness. The analysis of the cross-sectional images of the samples is not reasonable, because the thickness of the aggregates is comparable to the size of pixels and beam-hardening artefacts are dominant (figure 8). Therefore, for samples based on the filler with smallest particles (BASF CC carbonyl iron powder), only images obtained using optical microscopy will be shown below.

As follows from the dependencies in figure 6, it is quite realistic to interrupt the process of structuring of the very low concentrated composites ($\phi < \sim 0.5 \text{ vol.}\%$) by ‘freezing’ the liquid matrix during the first few minutes after switching on the magnetic field with a strength of several kA m^{-1} and there is no need to do it as a snap action. Such ‘freezing’ is realized by means of UV polymerization. This ‘freezing’ is realized by UV curing, which takes from a few seconds to a few minutes to cure the bulk specimen. The use of higher fields at very low concentrations or low fields at concentrations in the range approximately $0.5 \text{ vol.}\% < \phi < \sim 1 \text{ vol.}\%$ provides a potential opportunity to catch transition structures in the cured composite. Having provided the composite for a long enough time for structuring it is to be expected that equilibrium structures will appear regardless of the particle concentration and the applied field strength. In large fields, the aggregates will form relatively quickly, so their size should be regulated by the concentration

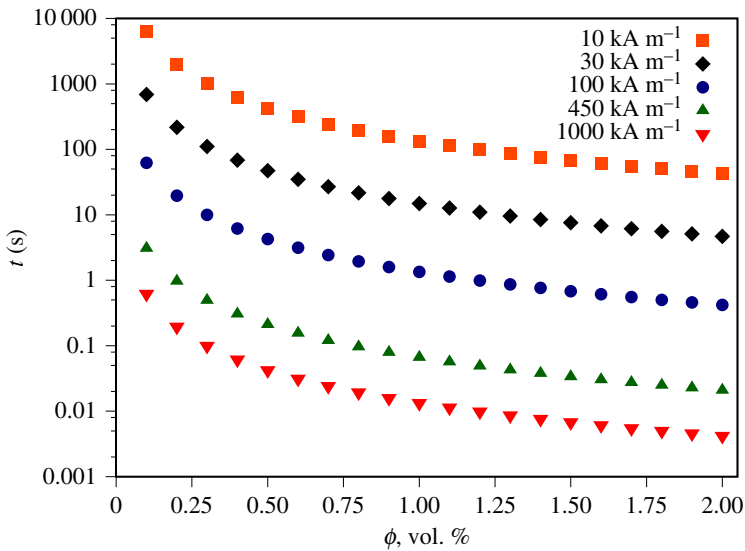


Figure 6. Dependence of structuring time t on the volume concentration of particles in the sample for various magnetic field strengths (the viscosity and magnetic permeability of the carrier medium are assumed to be $\eta = 9.77$ Pa s and $\mu_c = 1$, respectively). (Online version in colour.)

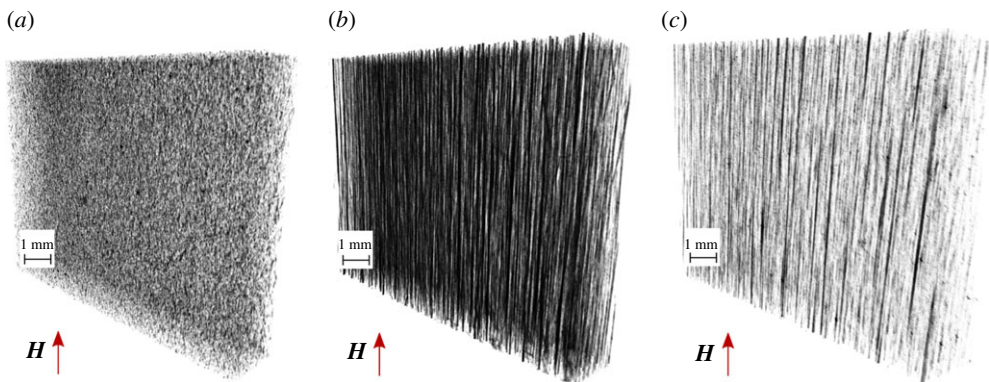


Figure 7. Reconstructed three-dimensional CT-images of a composite based on BASF CC carbonyl iron ($\phi \sim 0.15$ vol.%) patterned at: $H = 10$ kA m $^{-1}$ (a), $H = 100$ kA m $^{-1}$ (b) and $H = 450$ kA m $^{-1}$ (c). (Online version in colour.)

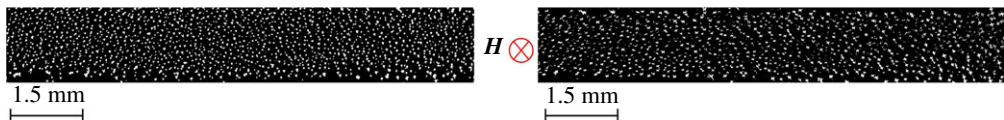


Figure 8. Examples of binarized images of cross-sections of samples presented in figure 7(b)—left and 7(c)—right. The beam hardening artefacts are comparable to the size of the cross-sections of the particle aggregates. (Online version in colour.)

and size of the filler particles. In general, it is reasonable to use the ratio of time given to particles for structuring within fabrication process t_p to structuring time t (equation (2.7)) as an evaluation criterion of the final microstructure of the composite. The time t_p includes polymerization time and can be taken in order of magnitude if its exact value is unknown. Such an assessment using ranges of values seems to us to be the most objective, since the actual concentration of particles in the composite is also unknown, and it may differ from the desired one. This is due to the fact

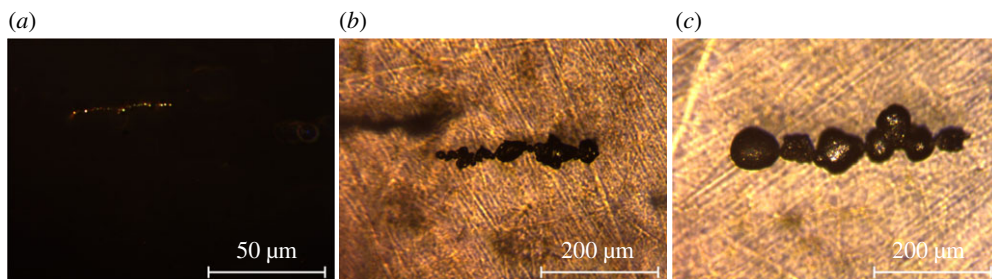


Figure 9. Microscopic images of short chains in patterned at $H = 10 \text{ kA m}^{-1}$ and $t_p/t \gg 1$ composites: (a) sample based on ~ 0.15 vol.% of BASF CC powder; (b) ample based on ~ 0.15 vol.% of ASC300 powder; (c) sample based on ~ 0.13 vol.% of Ni powder. (Online version in colour.)

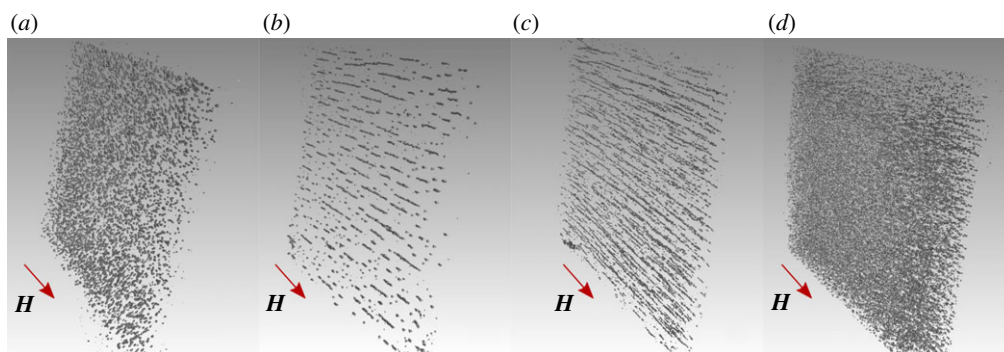


Figure 10. Reconstructed three-dimensional CT-images: (a) non-patterned, despite the applied field ($H = 10 \text{ kA m}^{-1}$), composite with ~ 0.13 vol.% of nickel microparticles, $t_p/t \ll 1$; (b) patterned at $H = 10 \text{ kA m}^{-1}$ and $t_p/t \gg 1$ composite with < 0.13 vol.% nickel microparticles; (c) patterned at $H = 10 \text{ kA m}^{-1}$ and $t_p/t \gg 1$ composite with ~ 0.15 vol.% of ASC300 iron microparticles; (d) patterned at $H = 10 \text{ kA m}^{-1}$ and $t_p/t \sim 1$ composite with ~ 1.6 vol.% of ASC300 iron microparticles. Notable is the shorter length of the chains in sample (d) than in sample (c), although the particle concentration in sample (d) is almost tenfold greater. (Online version in colour.)

that even small deviations in the number of particles in the volume unit will significantly change the concentration of the filler (equation (2.8)). Digital analysis of the μ CT-images allows one to determine the number of particles in the sample as *post factum*. However, this does not give any advantage in the choice of patterning parameters.

The approach discussed here was used to fabricate targeted patterned composites. The highlighted results of microstructure visualization of the obtained composites are presented and discussed below.

(b) Composites with short single chains

A short chain composite, i.e. a composite with chains which do not overlap it, can be obtained by using a very low particle concentration or, strictly speaking, a low particle number per volume unit (figures 9–11). However, it should be taken into account that for small fields, such as $\sim 10 \text{ kA m}^{-1}$, the ratio t_p/t should be much higher than unity. If this condition is not fulfilled for a small number of particles, the sample will not be structured (figure 10a). On the other hand, at higher concentrations one will also obtain short chains when the ratio t_p/t is close to unity (10c). When the field strength is greater than 30 kA m^{-1} , it is not technically possible to implement conditions $t_p/t \ll 1 \cap t_p/t \sim 1$ for the used materials, since it is impossible to realize instant

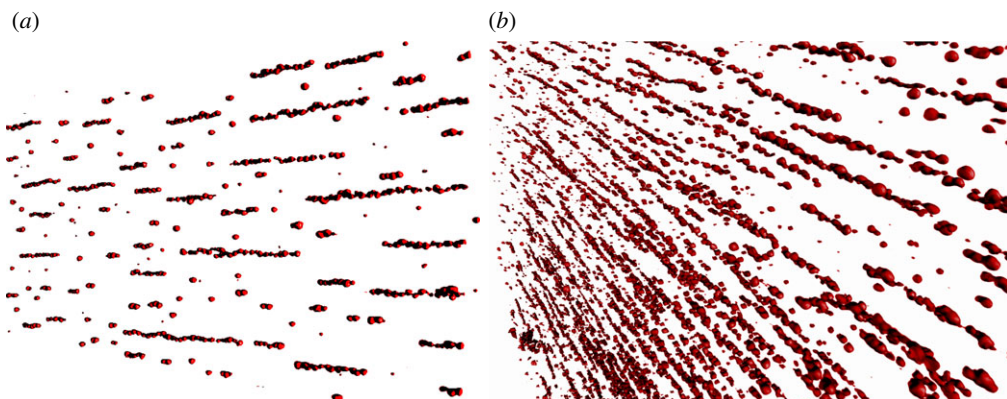


Figure 11. three-dimensional visualization (selected fragments) of the short chains: (a) a composite with $< 0.13\text{ vol.}\%$ nickel microparticles patterned at $H = 10\text{ kA m}^{-1}$ (figure 10b); (b) a composite with $\sim 0.15\text{ vol.}\%$ ASC300 iron microparticles (figure 10c) patterned at $H = 10\text{ kA m}^{-1}$. Condition $t_p/t \gg 1$ is fulfilled. Without scale. (Online version in colour.)

polymerization of the matrix. The increase of initial viscosity of the suspension or reduction of particle concentration is not so effective and, therefore, the best solution may be to use relatively low fields at $t_p/t \sim 1$ to obtain short chains.

Figure 9 demonstrates selected optical images of short chains in such composites. In figure 10 reconstructed three-dimensional CT-images of non-patterned and patterned at 10 kA m^{-1} specimens are shown. In addition, the figure 11 provides selected three-dimensional visualizations of composites with short chains. In addition to short chains, there are also individual particles in the sample volume. The influence of the magnetic field was insufficient to involve all the particles in the process of structuring, despite the fact that condition $t_p/t \gg 1$ is definitely fulfilled. In fact, time t_p was about 12 h during the manufacture of the particular sample with nickel microparticles patterned at $H = 10\text{ kA m}^{-1}$ and represented in figures 10c and 11a.

(c) Composites with thin long chain aggregates

Composites with long chains are samples in which the chain aggregates trend to overlap the specimen volume from one side to the other. Long aggregates consist of both thin single chains and several chains joined together, but their thickness does not significantly exceed the particle size. There are also a number of shorter aggregates similar to chains in the samples presented in §4b. To obtain composites with such a microstructure, it is necessary to use a weak and moderate magnetic field (approx. $10\text{--}100\text{ kA m}^{-1}$) and ensure that the condition $t_p/t \gg 1$ is met. The higher the particle concentration (within limits considered up to $2\text{ vol.}\%$), the denser the chain aggregates are. However, if $t_p/t \ll 1$, composites with short chains will be obtained (see §4b). Alternatively, higher magnetic fields ($> 100\text{ kA m}^{-1}$) at lower concentrations (up to $\sim 0.2\text{ vol.}\%$) can be used. But in the case of very low concentrations, it should be taken into account that the size effect may have a significant influence on the patterning. This issue is beyond the scope of this study. Obtaining non-ergodic structures is not to be expected, since, as already mentioned above, the condition $t_p/t \ll 1 \cap t_p/t \sim 1$ is not realizable for fields significantly greater than 10 kA m^{-1} . Selected microscopic images of composites with long chain aggregates are given in figure 12, while their three-dimensional microstructure is presented in figures 13 and 14. Note that sample (d) in figure 13 is identical in composition to sample (d) in figure 10. Moreover, a field of the same intensity was used for their patterning. The difference in the microstructure is obtained due to the different ratio t_p/t . In general, such samples are composites, the microstructure of which has similarity to that of the materials obtained and analysed in [15]: the lower the strength of the applied field, the more chains appear in the composite. The crucial difference is that in our study

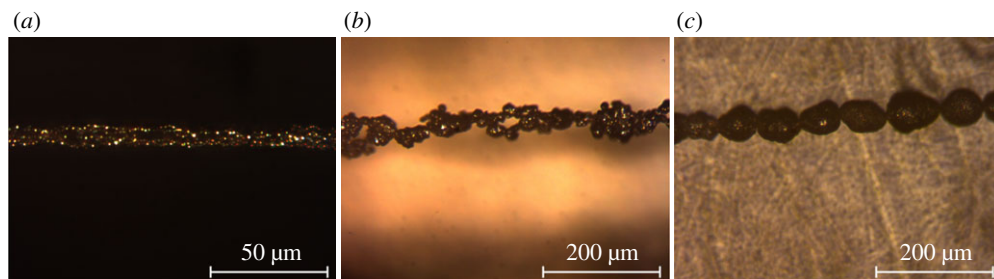


Figure 12. Microscopic images of long chains in patterned composites: (a) sample based on ~ 0.15 vol.% of BASF CC powder patterned at $H = 250 \text{ kA m}^{-1}$; (b) sample based on ~ 0.8 vol.% of ASC300 powder patterned at $H = 100 \text{ kA m}^{-1}$; (c) sample based on ~ 0.13 vol.% of Ni powder patterned at $H = 450 \text{ kA m}^{-1}$. For all samples, $t_p/t \gg 1$. (Online version in colour.)

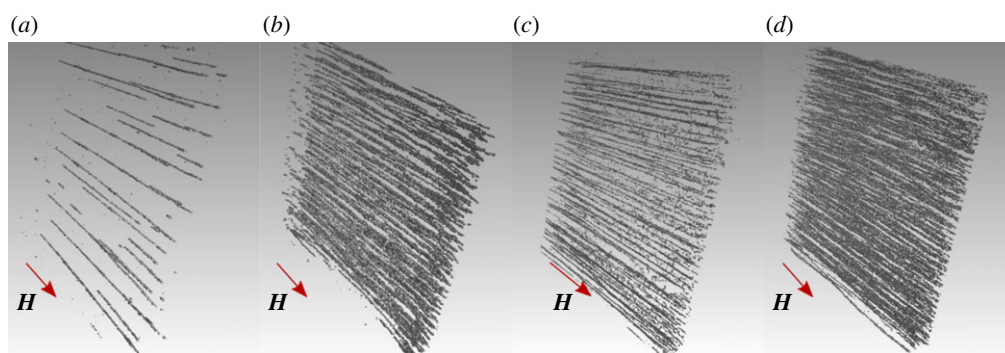


Figure 13. Reconstructed three-dimensional CT-images: (a) composite with < 0.13 vol.% of nickel microparticles patterned at $H = 450 \text{ kA m}^{-1}$ and $t_p/t \gg 1$; (b) composite with ~ 1.4 vol.% nickel microparticles patterned at $H = 10 \text{ kA m}^{-1}$ and $t_p/t \gg 1$; (c) composite with ~ 0.8 vol.% of ASC300 iron microparticles patterned at $H = 100 \text{ kA m}^{-1}$ and $t_p/t \gg 1$; (d) composite with ~ 1.6 vol.% of ASC300 iron microparticles patterned at $H = 10 \text{ kA m}^{-1}$ and $t_p/t \gg 1$. (Online version in colour.)

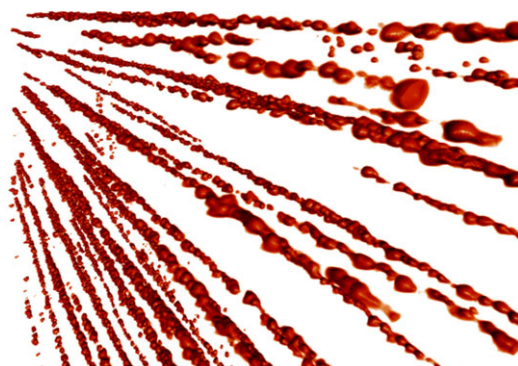


Figure 14. three-dimensional visualization (selected fragment) of the long chains in the composite with ~ 0.15 vol.% ASC300 iron microparticles patterned at $H = 100 \text{ kA m}^{-1}$. Condition $t_p/t \gg 1$ is fulfilled. Without scale. (Online version in colour.)

the polymerization process was initiated at a given point in time. Another feature is the mutual orientation of the magnetic field and gravity. In the current study, the magnetic field and gravity are perpendicular, while in [15] they are coaxial, so the chain aggregates observed by us do not have thickenings/thinnings at the ends.

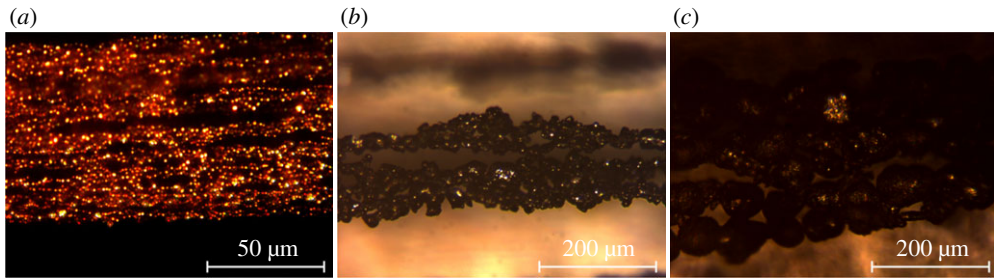


Figure 15. Microscopic images of thick chains in patterned composites: (a) sample based on ~ 0.8 vol.% of BASF CC powder patterned at $H > 450 \text{ kA m}^{-1}$; (b) sample based on ~ 0.8 vol.% of ASC300 powder patterned at $H = 450 \text{ kA m}^{-1}$; (c) sample based on ~ 1.4 vol.% of Ni powder patterned at $H = 450 \text{ kA m}^{-1}$. For all samples, $t_p/t \gg 1$. (Online version in colour.)

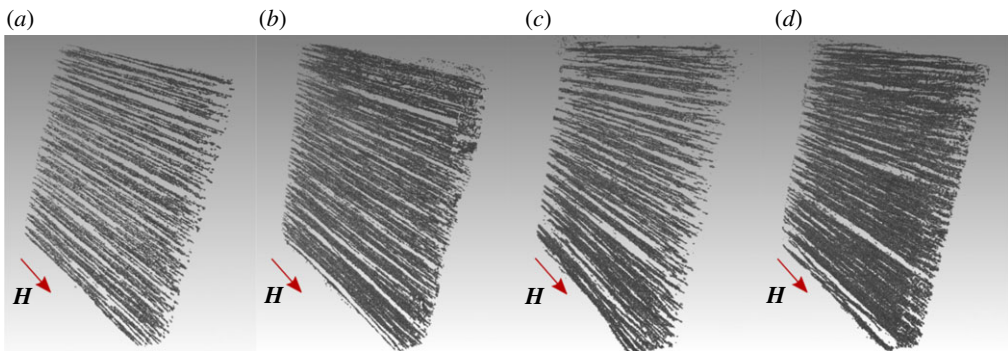


Figure 16. Reconstructed three-dimensional CT-images: (a) composite with ~ 1.4 vol.% of nickel microparticles patterned at $H = 450 \text{ kA m}^{-1}$ and $t_p/t \gg 1$; (b) composite with ~ 1.6 vol.% ASC300 iron microparticles patterned at $H = 100 \text{ kA m}^{-1}$ and $t_p/t \gg 1$; (c) composite with ~ 0.8 vol.% of ASC300 iron microparticles patterned at $H = 450 \text{ kA m}^{-1}$ and $t_p/t \gg 1$; (d) composite with ~ 1.6 vol.% of ASC300 iron microparticles patterned at $H = 450 \text{ kA m}^{-1}$ and $t_p/t \gg 1$. (Online version in colour.)

(d) Composites with thick chain/columnar aggregates

Technically speaking, there is a need for a precise criterion that determines when an aggregate is thin and when it should be considered columnar. To do this, one can use the method presented in [15,16]. Nevertheless, in the framework of this work we use only subjective judgement based on images of the microstructure without conducting corresponding quantitative digital analysis. The presence of thick chains is confirmed in particular by direct optical observations in the microscope. The differences between these aggregates and the thin chains are obvious, e.g. comparing figures 12 and 15.

It is quite obvious that composites with column aggregates (thick chains) should appear at high concentrations of particles and strong magnetic fields. Fields higher than 100 kA m^{-1} should be used for concentrations of at least ~ 1.6 vol.% and fields higher than $300\text{--}400 \text{ kA m}^{-1}$ for concentrations not less than ~ 0.8 vol.%. Within the framework of these conditions, the ratio t_p/t always will be much greater than unity. Thus, it is reasonable to assume that the structures obtained correspond to the equilibrium state. Selected microscopic images of composites with thick chains are shown in figure 15 and their three-dimensional microstructure is presented in figures 16 and 17.

The intermediate state of aggregation of chains into columns can be tubes or tube-like objects. We were unable to provide a state in which tubular structures could be observed in the matrix, as

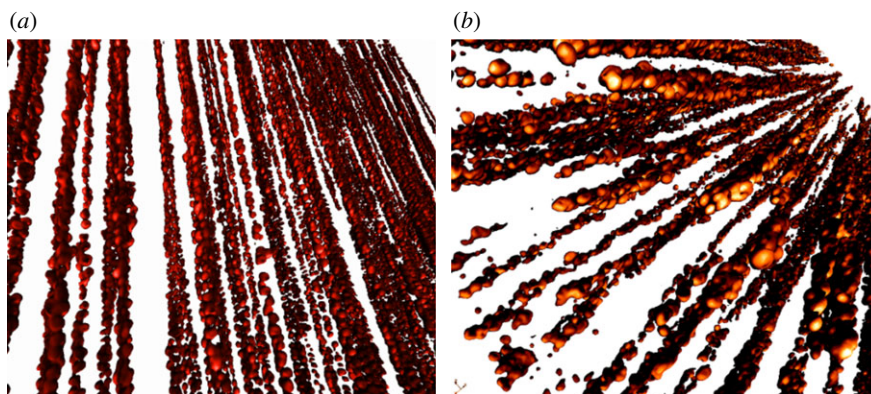


Figure 17. three-dimensional visualization (selected fragments) of the columnar structures: (a) composite with ~ 1.4 vol.% of nickel microparticles patterned at $H = 450 \text{ kA m}^{-1}$ (figure 16a); (b) composite with ~ 1.6 vol.% ASC300 iron microparticles patterned at $H = 450 \text{ kA m}^{-1}$ (figure 16c). Condition $t_p/t \gg 1$ is fulfilled. Without scale. (Online version in colour.)

was provided in a composite containing comparable particle concentration but fabricated under curing with uncontrollable initiation [18]. One may expect their appearance, when ‘freezing’ the structuring process in one of its intermediate states, which was not possible to realize under conditions used in the current study. We also assume that the appearance of tubular structures observed in studies [16,18] may be associated with inhomogeneous polymerization of the composite due to the influence of the filler particles on the catalyst and, consequently, on the polymerization process.

5. Summary and outlook

We have demonstrated the possibility of targeted patterning of low-concentrated magnetic polymeric composites. In contrast to previous studies, the process of polymerization of the composite was initiated at a specific point in time, an equilibrium state of the composite microstructure to be reached. On the other hand, for specimens with a certain composition it was possible to ‘freeze’ the non-ergodic state in a controllable way, for example to obtain short chains at particle concentrations, potentially resulting in the appearance of thick column aggregates. These results are the basis for the development of engineering approaches of targeted patterning, which allows one to obtain a material with the desired microstructure by selecting specific parameters of external stimuli and components of the composite.

We did not directly address the issue of fine-size effects, which undoubtedly plays an important role in the processes of microstructure formation and should be addressed in future works. In addition, attention should be paid to composites with a higher concentration of filler. However, it will require the use of higher computational power and special algorithms for the reconstruction of μ CT-data.

As an additional factor that can significantly affect the final morphology of structured magnetic composites, a shear flow can be considered. It is possible to directly apply shear strain to the specimen during the curing process. On the other hand, a rotating magnetic field can be used (e.g. [24]). In these cases, the size and morphology of the final structures in the polymer will be determined by competition between structuring processes due to magnetic interaction and disaggregation due to the hydrodynamic forces. The study of the microstructure of such composites will also contribute to a deeper understanding of the physics of rheological effects in magnetic suspensions.

Data accessibility. This article has no additional data.

Competing interests. The author declares that he has no competing interests.

Funding. The study was supported by Deutsche Forschungsgemeinschaft (DFG) under grant no. BO 3343/2-1 within SPP1681 and DFG-RFBR PAK907.

Acknowledgements. The authors thank Prof. Stefan Odenbach for providing laboratory facilities of the Chair of Magnetofluidynamics, Measuring and Automation Technology at TU Dresden. Malte Schümman's (TU Dresden) technical assistance and advice with μ CT and Gennady Stepanov's (GNIChTEOS, Moscow) advice with chemicals are acknowledged.

References

1. Odenbach S (ed.) 2009 *Colloidal magnetic fluids*, vol. 763. Lecture Notes in Physic. Berlin, Heidelberg: Springer.
2. Bossis G, Volkova O, Laci S, Meunier A. 2002 *Magnetorheology: fluids, structures and rheology*. In *Ferrofluids. Magnetically controllable fluids and their applications* (ed. S Odenbach). Lecture Notes in Physic, vol. 594. Berlin, Heidelberg: Springer.
3. Thévenot J, Oliveira H, Sandre O, Lecommandoux S. 2013 Magnetic responsive polymer composite materials. *Chem. Soc. Rev.* **42**, 7099–7116. (doi:10.1039/c3cs60058k)
4. Odenbach S. 2016 Microstructure and rheology of magnetic hybrid materials. *Arch. Appl. Mech.* **86**, 269–279. (doi:10.1007/s00419-015-1092-6)
5. Iskakova L, Romachnuk A, Zubarev A. 2006 Phase and structural transformations in magnetorheological suspensions. *Physica A* **366**, 18–33. (doi:10.1016/j.physa.2005.10.051)
6. Lopez-Lopez MT, Kuzhir P, Zubarev A. 2014 Effect of drop-like aggregates on the viscous stress in magnetic suspensions. *J. Non-Newtonian Fluid Mech.* **208–209**, 53–58. (doi:10.1016/j.jnnfm.2014.04.001)
7. Nowak J, Borin D, Haefner S, Richter A, Odenbach S. 2017 Magnetoviscous effect in ferrofluids diluted with sheep blood. *J. Magn. Magn. Mater.* **442**, 383–390. (doi:10.1016/j.jmmm.2017.07.029)
8. Tao R. 2001 Super-strong magnetorheological fluids. *J. Phys.: Condens. Matter* **13**, R979–R999. (doi:10.1088/0953-8984/13/50/202)
9. Bossis G, Iskakova L, Kostenko V, Zubarev A. 2011 Kinetics aggregation of magnetic suspensions. *Physica A* **390**, 2655–2663. (doi:10.1016/j.physa.2011.02.044)
10. Bossis G, Lancon P, Meunier A, Iskakova L, Kostenko V, Zubarev A. 2013 Kinetics of internal structures growth in magnetic suspensions. *Physica A* **392**, 1567–1576. (doi:10.1016/j.physa.2012.11.029)
11. Furst E, Gast A. 2000 Micromechanics of magnetorheological suspensions. *Phys. Rev. E* **61**, 6732–6739. (doi:10.1103/PhysRevE.61.6732)
12. Ivaneyko D, Toshchevnikov V, Saphiannikova M. 2015 Mechanical properties of magneto-sensitive elastomers: unification of the continuum-mechanics and microscopic theoretical approaches. *Soft Matter* **11**, 7627–7638. (doi:10.1039/C5SM01761K)
13. Zubarev AY., Chirikov DN, Borin DYu, Stepanov GV. 2016 Hysteresis of the magnetic properties of magnetic gels. *Soft Matter* **12**, 6473. (doi:10.1039/C6SM01257D)
14. Borin D, Günther D, Hintze C, Heinrich G, Odenbach S. 2012 The level of cross-linking and the structure of anisotropic magnetorheological elastomers. *J. Magn. Magn. Mater.* **324**, 3452–345. (doi:10.1016/j.jmmm.2012.02.063)
15. Borbáth T, Günther S, Borin D, Gundermann T, Odenbach S. 2012 X-ray microCT analysis of magnetic field-induced phase transitions in magnetorheological elastomers. *Smart Mater. Struct.* **21**, 105018. (doi:10.1088/0964-1726/21/10/105018)
16. Günther D, Borin D, Günther S, Odenbach S. 2012 X-ray micro-tomographic characterization of field-structured magnetorheological elastomers. *Smart Mater. Struct.* **21**, 015005. (doi:10.1088/0964-1726/21/1/015005)
17. Schümman M, Borin DY, Huang S, Auernhammer GK, Müller R, Odenbach S. 2017 A characterisation of the magnetically induced movement of NdFeB-particles in magnetorheological elastomers. *Smart Mater. Struct.* **26**, 095018. (doi:10.1088/1361-665X/aa788a)
18. Borin D, Odenbach S, Iskakova L, Zubarev A. 2018 Non-ergodic tube structures in magnetic gels and suspensions. *Soft Matter* **14**, 8537–8544. (doi:10.1039/C8SM01456F)
19. Jones TB. 1995 *Electromechanics of particles*. Cambridge, UK: Cambridge University Press.

20. Fermigier M, Gast A. 1992 Structure evolution in a paramagnetic latex suspension. *J. Colloid Interface Sci.* **154**, 522–539. (doi:10.1016/0021-9797(92)90165-1)
21. Zubarev A. 2001 On the theory of condensation phase transitions in magnetic and electrorheological suspensions. *Colloid J.* **61**, 338–343.
22. Shevchenko N, Boden S, Eckert S, Borin D, Heinze M, Odenbach S. 2013 Application of X-ray radioscopic methods for characterization of two-phase phenomena and solidification processes in metallic melts. *Eur. Phys. J. Spec. Top.* **220**, 63–77. (doi:10.1140/epjst/e2013-01797-y)
23. Périgo EA, Weidenfeller B, Kollár P, Füzér J. 2018 Past, present, and future of soft magnetic composites. *Appl. Phys. Rev.* **5**, 031301. (doi:10.1063/1.5027045)
24. Melle S, Calderón G, Rubio M, Fuller G. 2003 Microstructure evolution in magnetorheological suspensions governed by Mason number. *Phys. Rev. E* **68**, 041503. (doi:10.1103/PhysRevE.68.041503)